doi:10.14311/ppt.2025.1.1
Plasma Physics and Technology **12**(1):1–9, 2025

NUMERICAL STUDIES OF PLASMA EMISSION IN A MEGA JOULE PLASMA FOCUS USING LEE CODE

M. A. Malek[a,*], M. N. Huda[a], M. K. Islam[b], M. Akel[c], S. Lee[d,e,f]

[a] *Physics Discipline, Khulna University, Khulna 9208, Bangladesh*
[b] *Plasma Physics Division, Atomic Energy Center, Dhaka 1000, Bangladesh*
[c] *Department of Physics, Atomic Energy Commission, P. O. Box 6091, Damascus, Syria*
[d] *Institute for Plasma Focus Studies, 32 Oakpark Drive, Chadstone, VIC 3148, Australia*
[e] *INTI International University, 71800 Nilai, Malaysia*
[f] *University of Malaya, 50603 Kuala Lumpur, Malaysia*
[*] malekphy@gmail.com

Abstract. In this paper, plasma emissions (radiative recombination, bremsstrahlung, and line radiation) from a mega-joule plasma focus (PF1000) device is studied using the Lee code for nitrogen (N_2), oxygen (O_2) and argon (Ar) gases with pressure variation in the range of (0.05–2.5) Torr. Ion density, plasma velocity, pinch temperature, Joule heating, peak current, and minimum pinch radius are also obtained with pressure change for each of the gases. It is found that the line radiation is predominant compared to bremsstrahlung radiation and radiative recombination for each gas. At the optimum pressure, the maximum line radiations are found as: 3.9 kJ (91 % of total emissions) at 0.945 Torr N_2, 6.2 kJ (85 % of total emissions) at 0.6 Torr O_2 and 30 kJ (97 % of total emissions) at 0.23 Torr Ar, respectively. The minimum pinch radius ($r_{\min}$) and consequent ion densitiy (N_i) of these gases are computed at their corresponding optimum pressures. It is found that the $r_{\min}$ (0.13 cm) of Ar is 10-fold smaller than N_2 (1.25 cm) while it is 6-fold smaller in O_2 (0.82 cm). This smallest minimum pinch radius of Ar produces the dominating ion density (71×10^{23} m^{-3}) compared to N_2 (3×10^{23} m^{-3}) and O_2 (5×10^{23} m^{-3}) gases resulting the highest line radiation is found for Ar. The sharp dropping of the pinch radius of Ar plasma followed by the greatest plasma emission (line) shows the strong evidence of radiatively-enhanced compressions.

Keywords: Gas pressure, Pinch radius, radiatively-enhanced compressions, Plasma emission, PF1000.

1. Introduction

Plasma focus (PF) device is a high-power self-generated electromagnetic accelerator which can produce and compress plasma in a thin filament in front of the inner electrode (anode) [1–3]. This machine is studied as an intense source of X-rays for its potential applications in industries such as medical use [4–9], micro-machining [10, 11], and lithography [12–14]. The characteristics of plasma emission from the PF strongly depend on the operating principles and parameters (e.g., composition of filling gas and pressure, operating energy, electrode's materials and geometry, discharge current, anode polarity etc.). Especially, the filling gas composition, puffing pressure, and discharge current have the strongest influence on plasma emission [15–18]. A large number of research articles are published on experimentally studied yields (X-ray, neutron, ion, and electron beams) from PF devices. Several of them are focused on the X-ray yield enhancement through changing the insulator sleeve length and material, varying the plasma density within the pinch (at anode top) by way of gas puffing or using tapered anode and others are correlated the electrode geometry (material, shape, and dimension) with soft X-ray emission [19–21].

Presently, the experimentally organized trial and error technique to find the optimized arrangement of a PF for maximum plasma emission is very difficult, highly time-consuming, and needs finance. It can be accomplished if a reliable focus model and consequent code of simulation is developed and used, which can be able to predict realistically the radiation yields from a PF. The Lee code is one of the prominent codes in which the electrical circuit and plasma focus dynamics, thermodynamics along with radiation are coupled [22, 23]. This code realistically simulates the experimental results from a PF by only matching the computed current waveform with the measured one [24]. It is convenient to perform scaling studies phenomenological of any low energy to high energy PF devices using the code [25]. Previously, it is used to simulate different PF devices, including UNU/ICTP PFF [26, 27], NX2 [28, 29], NX1 [28], [30], and Filippov-type PF DENA [31]. In several publications, the Lee code is used to obtain the optimum combination of puffing gas pressure, anode configuration with either a fixed cathode radius or constant radius ratio to enhance soft X-ray emission (SXR) from PF devices [32, 33].

Plasma emission with pressure variation has been

studied numerically in the spherical PF device for N_2 and Ne gases [34]. A numerical study on PF1000 was conducted previously to find the optimized characteristic SXR yield for Ne gas with pressure change [35]. In this present work, we extend the numerical experiments to study plasma emission with change in pressure for N_2, O_2, and Ar gases using the Lee code (version: RADPFV5.15). The minimum plasma pinch column radius, ion density, pinch plasma temperature, peak discharge current, and plasma velocity are also obtained and correlated with plasma emission for each of the gases.

2. The Lee Code Configuration for Numerical Experiment

In the Lee code, the following power equations are considered, respectively, to calculate Bremsstrahlung, Recombination, Line radiation, and Joule heating, generated from the pinch plasma column in a PF device [36]:

Bremsstrahlung radiation power:

$$\frac{\mathrm{d}Q_{\mathrm{br}}}{\mathrm{d}t} = -1.6 \times 10^{-40} N_i^2 Z_{\mathrm{eff}}^3 (\pi r_{\mathrm{min}}^2) Z_{\mathrm{max}} T^{0.5} \quad (1)$$

Line radiation power:

$$\frac{\mathrm{d}Q_{\mathrm{ln}}}{\mathrm{d}t} = \frac{-5.92 \times 10^{-35} N_i^2 Z_{\mathrm{eff}}^5 (\pi r_{\mathrm{min}}^2) Z_{\mathrm{max}}}{T^{0.5}} \quad (2)$$

Radiative recombination power:

$$\frac{\mathrm{d}Q_{\mathrm{rec}}}{\mathrm{d}t} = \frac{-4.6 \times 10^{-31} N_i^2 Z_{\mathrm{eff}} Z_n^4 (\pi r_{\mathrm{min}}^2) Z_{max}}{T} \quad (3)$$

Joule heating power:

$$\frac{\mathrm{d}Q_{\mathrm{Joule}}}{\mathrm{d}t} = 1300 \times \frac{Z_{\mathrm{eff}} \times Z_{\mathrm{max}}}{\pi r_{\mathrm{min}}^2} I^2 T^{-1.5} \quad (4)$$

Hence, it is clear from Eqs. (1)–(4) that ion number density (N_i), effective charge number (Z_{eff}), atomic number of gas (Z_n), minimum pinch column radius (r_{min}), pinch column length (Z_{max}), pinch plasma temperature (T), pinch current (I) are strongly co-related with plasma emission in a PF device.

The PF1000 is a ~1 MJ PF device located in Poland. Here, the code is configured with the capacitor bank characteristics, tube dimensions, and operating voltage and pressure (Table 1) of the standard PF1000 [37].

The model parameters such as mass swept-up factor in axial phase, $f_{\mathrm{m}} = 0.13$, effective current factor in axial phase, $f_{\mathrm{c}} = 0.7$, mass swept-up factor in radial phase, $f_{\mathrm{mr}} = 0.35$, and effective current factor in radial phase, $f_{\mathrm{cr}} = 0.65$ have been obtained by fitting the computed and measured current waveforms at 3.5 Torr deuterium in PF1000 [37]. This set of model parameters and the above tabulated configuration of the PF device are used for our present series of numerical experiments for different gases [38–40].

3. Results and Discussions

The plasma emission is computed from PF1000 device using the Lee code for N_2, O_2, and Ar gases with pressure variation in the range of (0.05–2.5) Torr. Finally, we obtain the optimum pressure at which the plasma emission is maximum from the device for these gases. The peak discharge current (I_{peak}), magnetic piston speed (v_{p}) along with some plasma pinch properties such as maximum pinch plasma temperature (T_{max}), minimum pinch radius, ion density, joule heating energy for these gases are also computed and only the results for N_2 gas are tabulated (Table 2). The findings for the other two gases (O_2 and Ar) are discussed with graphs in this paper.

In a plasma focus, the Coulomb interactions between ions and electrons are responsible for bremsstrahlung radiation while the radiative recombination is emitted by confining of a free electron with an ion. The computed Joule heat, bremsstrahlung radiation, line radiation, and radiative recombination as a function of time from start of radial phase in PF1000 for Ar and N_2 gases are presented in Figs 1 and 2, respectively.

The lose energy due to dropping a bound electron from the higher ionic energy state to a lower state emits as line radiation in the PF device.

The figures (Figs. 3–5) show the computed bremsstrahlung radiation (Q_{br}), line radiation (Q_{ln}), and radiative recombination (Q_{rec}) as a function of pressure in PF1000 for N_2, O_2, and Ar gases. The maximum bremsstrahlung radiations are found as 49.24 J at 0.827 Torr N_2, 72.69 J at 0.6 Torr O_2, and 53.34 J at 0.127 Torr Ar (Fig. 3).

While, for the peak values of the recombination radiations are obtained as 355.07 J at 0.866 Torr N_2, 1.0 kJ at 0.6 Torr O_2, and 1.5 kJ at 0.127 Torr Ar (Fig. 4). It is noticed that the radiative recombination energies for O_2 and Ar are comparable but about 3-times greater in N_2 plasma and it is higher than bremsstrahlung radiation for each of the gases. The utmost line radiations (Fig. 5) 3.9 kJ for N_2, 6.2 kJ for O_2, and 30 kJ for Ar are computed at the optimum pressures of 0.945 Torr, 0.6 Torr, and 0.23 Torr, respectively. It is clear from these curves that the optimum value of line radiation for each gas is the greatest than the other types of radiation (bremsstrahlung and recombination). Comparing the above radiations, it is noticed that the line radiations for N_2, O_2, and Ar are 91 %, 85 %, and 97 % of the corresponding total plasma emission, respectively.

The figures (Figs. 3–5) also demonstrate that the increase in gas pressure indicates an increase in plasma emission in the beginning until getting some optimum gas pressure point for each of the gases. Beyond this point, the increase in gas pressure reduces the emission from PF1000 device in terms of bremsstrahlung radiation, line radiation, and radiative recombination. Some of the basic reasons for which the plasma emission varies with pressure in a PF device are given

Bank parameters:	Static inductance, L_0	33.5 nH
	Capacitance, C_0	1332 μH
	Stray resistance, r_0	6.1 mΩ
Tube parameters:	Cathode radius, b	16 cm
	Anode radius, a	11.55 cm
	Anode length, z_0	60 cm
Operating parameters:	Charging voltage, V_0	27 kV
	Gas pressures,P_0	(0.05–2.5) Torr

Table 1. Device parameters of the standard PF1000 for our numerical experiments.

P_0 (Torr)	I_{peak} (kA)	$T_{\max}$ ($\times 10^6$)	$r_{\min}$ (cm)	v_{p} (cmμs^{-1})	N_i (10^{23} m^{-3})	Q_{br} (J)	Q_{rec} (J)	Q_{ln} (J)	Q_{Joule} (J)
0.05	1291	18.2	2.12	28.3	0.06	0.20	0.22	0.41	0.50
0.10	1465	11.7	2.02	22.5	0.13	0.85	1.40	3.30	1.63
0.127	1525	9.7	1.93	20.8	0.19	1.46	2.92	7.56	2.67
0.135	1541	9.3	1.91	20.3	0.20	1.68	3.53	9.34	3.03
0.20	1638	6.8	1.82	17.7	0.33	4.06	11.66	36.09	6.75
0.23	1671	6.2	1.80	16.9	0.39	5.40	17.31	56.57	8.71
0.30	1731	4.9	1.77	15.3	0.53	9.32	36.97	134.44	14.27
0.40	1794	3.9	1.72	13.8	0.75	16.73	84.42	346.37	24.47
0.50	1844	3.2	1.65	12.6	1.01	26.52	163.68	742.86	38.14
0.60	1884	2.7	1.57	11.6	1.38	39.08	288.56	1432.73	57.17
0.70	1918	2.6	1.47	10.8	1.78	41.15	263.45	2050.25	63.76
0.80	1946	2.3	1.34	10.2	2.47	48.55	336.94	3140.04	87.69
0.827	1953	2.2	1.30	10.1	2.68	49.24	349.28	3409.46	95.32
0.866	1963	2.2	1.27	9.9	2.95	48.46	355.08	3706.40	106.94
0.945	**1981**	**2.0**	**1.25**	**9.5**	**3.0**	**41.85**	**327.26**	**3872.05**	**130.67**
1.00	1992	1.9	1.26	9.3	3.47	35.71	291.38	3720.52	144.83
1.50	2073	1.2	1.48	7.7	3.75	6.29	69.73	1382.78	252.11
2.00	2127	0.8	1.57	6.6	4.44	0.98	14.53	393.05	438.50
2.50	2166	0.6	1.57	5.8	5.59	0.16	3.25	116.27	731.71

Table 2. The computed results for N_2 gas in the pressure range (0.05–2.5) Torr at 27 kV in PF1000.

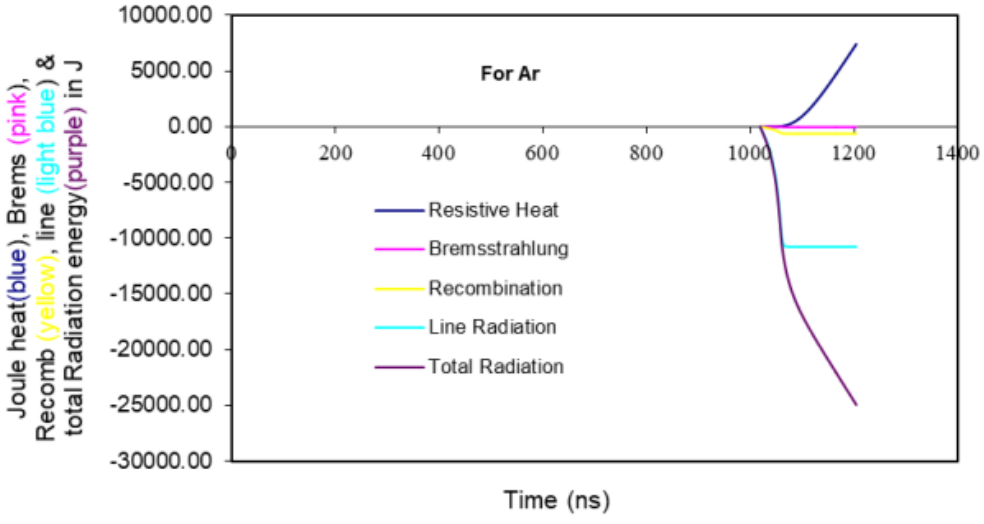

Figure 1. Heat and radiation emission from PF1000 device at 0.23 Torr Ar from start of radial phase.

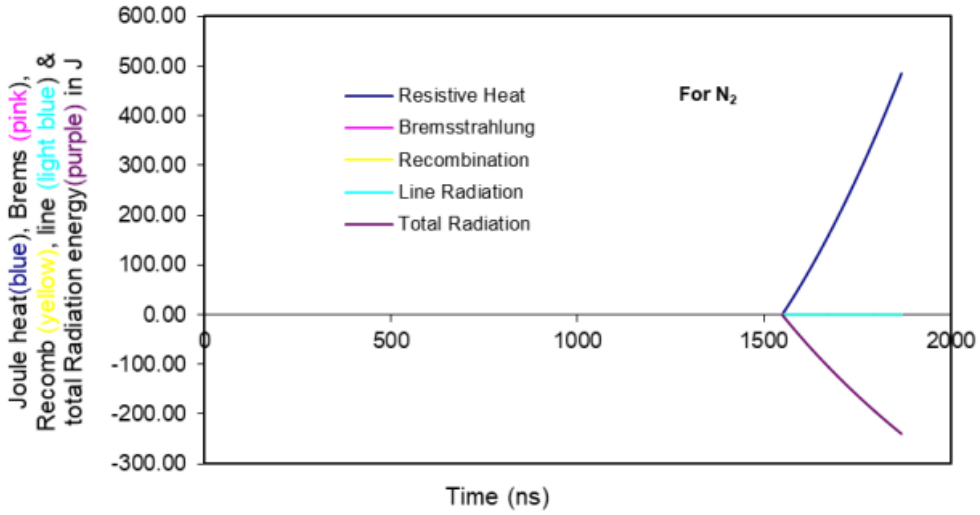

Figure 2. Heat and radiation emission from PF1000 device at 0.945 Torr N_2 from start of radial phase.

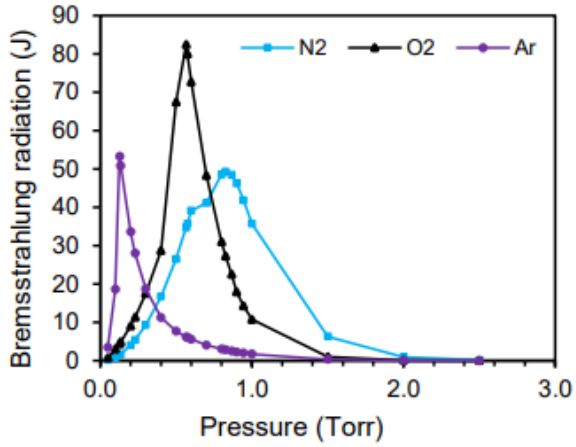

Figure 3. Bremsstrahlung radiadion for N_2, O_2, and Ar.

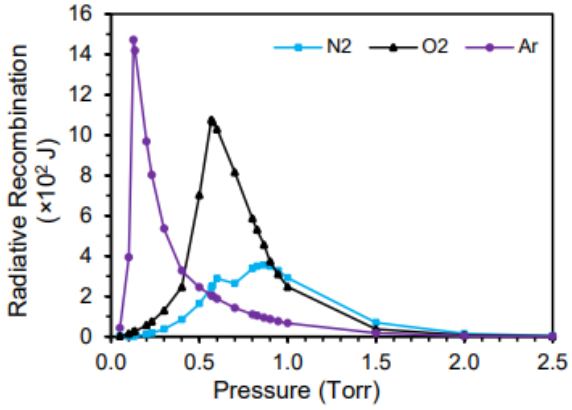

Figure 4. Radiative recombination for N_2, O_2, and Ar.

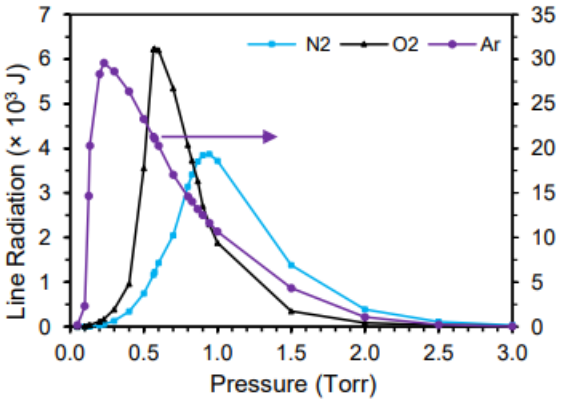

Figure 5. Line radiation for N_2, O_2, and Ar.

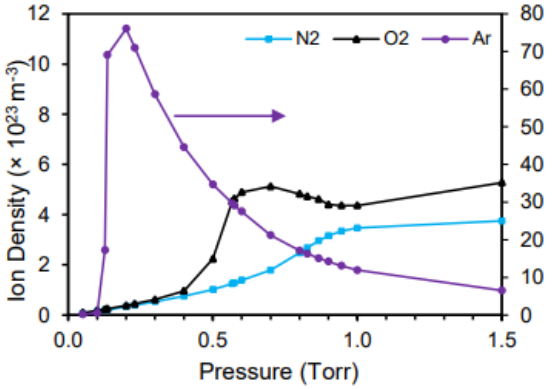

Figure 6. Ion densities for N_2, O_2, and Ar.

below.

In our study, we see that the ion density in pinch plasma is increasing with increasing gas pressure (Fig. 6), which increases the plasma emission. It increases continuously with the increase in gas pressure for each of the gases but for Ar, there is a peak ($76 \times 10^{23}\,\mathrm{m}^{-3}$) at 0.20 Torr (Fig. 6) and then it starts to reduce with further pressure increase.

While, N_i for N_2 increases gradually up to $3.47 \times 10^{23}\,\mathrm{m}^{-3}$ at 1.0 Torr and after that its increase rate becomes slow. In the case of O_2, it reaches to

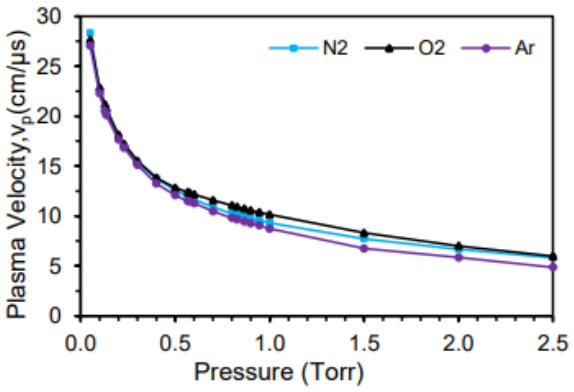

Figure 7. Plasma sheath velocities for N_2, O_2, and Ar.

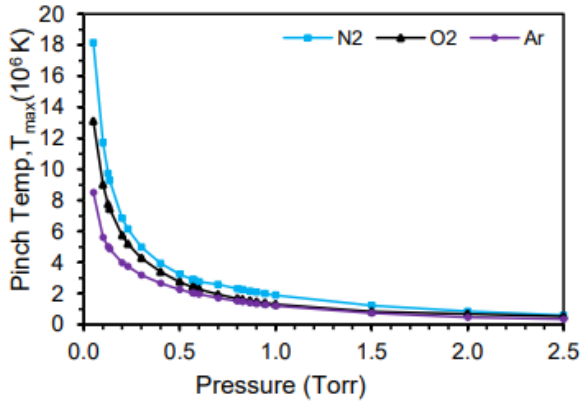

Figure 8. Pinch temperature for N_2, O_2, and Ar.

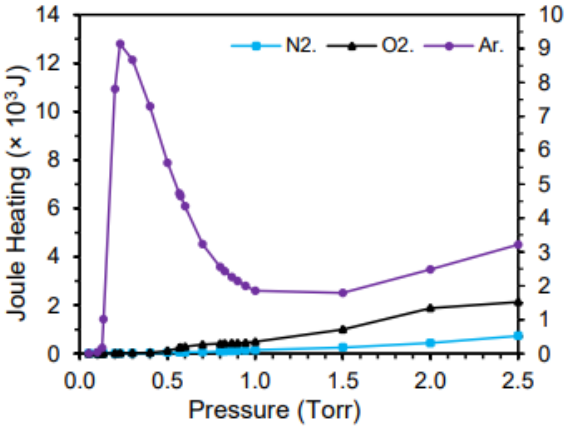

Figure 9. Joule heating for N_2, O_2, and Ar.

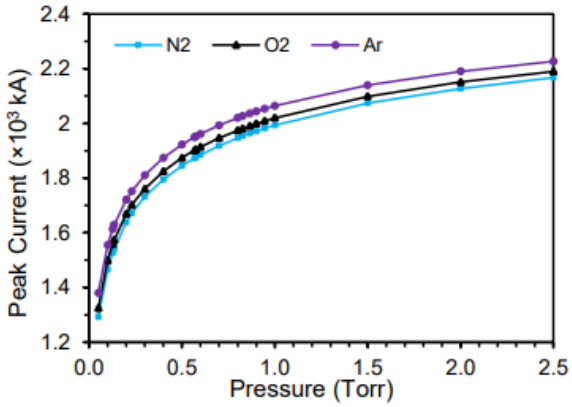

Figure 10. Peak current for N_2, O_2, and Ar.

$5.12 \times 10^{23}\,\mathrm{m}^{-3}$ at 0.7 Torr sharply and then starts to decrease with pressure rise until $4.36 \times 10^{23}\,\mathrm{m}^{-3}$ at 1.0 Torr. The optimum pressure for ion density and line radiation are very close to one another for each of the gases (Fig. 5 and Fig. 6) and hence, N_i has a strong effect on line radiation in pinch plasma which is the plasma dominating emission.

These curves of v_p and T_max for each of the gases are following the similar pattern in the pressure range of (0.05–2.5) Torr. The magnetic piston (plasma sheath) speed (Fig. 7) accordingly the maximum pinch temperature (Fig. 8) reduces with increasing gas pressure, which eventually decreases the compression of pinch plasma. The decrease in v_p with pressure increasing leads to a reduce in T_max. Both peaks v_p and T_max for N_2, O_2, and Ar gases are found at 0.05 Torr those are $28.30\,\mathrm{cm}\mu\mathrm{s}^{-1}$, $27.61\,\mathrm{cm}\mu\mathrm{s}^{-1}$, and $27.04\,\mathrm{cm}\mu\mathrm{s}^{-1}$, respectively and 18.2×10^6 K, 13.10×10^6 K, and 8.50×10^6 K, respectively.

At low pressure, the effect of the increase in ion density on plasma emission is stronger than the effect of the decrease in plasma velocity and temperature. Therefore, the plasma emissions are increasing with gas pressure until some optimum point and after this, further increasing the gas pressure, even though the ion density is increasing, the radiation yield starts to decrease, now the effect of decrease in plasma v_p and T_max is stronger on plasma emission.

Increasing gas pressure which eventually leads to an increase in Joule heating for all gases (Fig. 9). But for Ar, we look that the Joule heating energy goes to the maximum (9.1 kJ) at the pressure of 0.23 Torr and after that it starts to decrease with further pressure increase. For N_2 and O_2 gases, the rise in gas pressure results in increasing Joule heating continuously. An increase in gas pressure which leads to a rise peak current for each of gases in the device (Fig. 10). This rising rate is higher in the pressure range of (0.05–1.0) Torr compared to the increasing rate in the range of (1.5–2.5) Torr.

Due to electromagnetic compression (pinching) hot and dense plasmas are staging onto the anode top for very short time (few ns) which is the source of plasma emission (line and continuum) and then collapse for instabilities. During this compression, plasma gains internal energy from Joule heating requiring a bigger equilibrium pinch radius whilst it loses energy through plasma emission oppose this trend. When this emission exceed the Joule heating energy, the excess emission energy reduces the kinetic pressure (resisting) force whilst the magnetic piston continuously exerts a squeezing force in radially inward direction. If this cooling effect for plasma mission is sufficiently large,

then it leads to a very sharp drop in pinch radius (principal sign of radiatively-enhanced compression) and it might be a very far lesser than envisaged in the case of just the electromagnetic compression (pinch) [36]. In general, the presence and strength of plasma radiative compression depend on the initial values of radius, density, and temperature of a pinched column.

The reason for this is the radial velocity of compression depends on the plasma emission. So, when the initial value of plasma density is higher and temperature is smaller (assuming optically thin state), the plasma emission will be higher and radial compression faster because of the feedback type of relations–higher radiation emission leads to higher compression, while higher compression leads to higher radiation emission and so on (at least until an optically thick state is reached).

Moreover, there are other effects/phenomena during plasma-focus discharges which should also influence the compression of plasma pinch and achieved values of pinch radius, density, and temperature (and thus achieved maximum compression state) – they are not occur during discharges and influence radial compression of plasma pinch. Especially changes in the mass sweeping and current flow prior and during a plasma pinch formation (due to different possible effects occurring in an experimental chamber) – described with the model parameters, changes in the electric operation of a device – described with the total inductance and resistance of a device changes in the plasma compressibility – described with the total specific heat ratio of ionized gases, changes in the flow of current through pinch – due to changes in the Spitzer resistivity and changes in the time of stability of a pinch – due to changes in the time of propagation of small disturbances across a plasma column [41].

In our present numerical experiments, it is found that the minimum pinch radii for Ar, N_2, and O_2 plasmas reduce, consequently the total plasma emissions increases with pressure increase up to certain values. After these points, the plasma emissions start to reduce accordingly the rmin increases with further increasing pressure. At the optimum pressure of 0.945 Torr N_2, the $r_{\min}$, $T_{\max}$, and N_i are found to be 1.25 cm, 2.0×10^6 K, and 3.0×10^{23} m^{-3}, respectively, with the maximum total plasma emission of 4.2 kJ while for O_2, the peak total emission is found 7.3 kJ with 4.89×10^{23} m^{-3}, 3.0×10^6 K and 0.82 cm at the optimum pressure of 0.6 Torr (Fig. 11). In the case of Ar, the lowest $r_{\min}$ (0.10 cm) is found at 0.15 Torr with N_i (83×10^{23} m^{-3}), $T_{\max}$ (4.63×10^6 K), and total emission 25 kJ. But, the highest total emission (30 kJ) is obtained at 0.23 Torr with $r_{\min}$ (0.13 cm), N_i (71×10^{23} m^{-3}), and $T_{\max}$ (3.75×10^6 K). Here, we notice inequality relations in $r_{\min}$: $r_{\min}(N_2) > r_{\min}(O_2) > r_{\min}$ (Ar), in N_i : $N_i(\mathrm{Ar}) > N_i(O_2) > N_i(N_2)$, $T_{\max}$: $T_{\max}(\mathrm{Ar}) > T_{\max}(O_2) > T_{\max}(N_2)$, and consequently in total plasma emission (Q_{total}) : $Q_{\text{total}}(\mathrm{Ar}) > Q_{\text{total}}(O_2) > Q_{\text{total}}(N_2)$. That means, the reduction in $r_{\min}$ an increase in ion density resulting the higher up the plasma emission. We also observe the variations of radial trajectories (Fig. 12 and 13) for N_2, O_2, and Ar at their corresponding optimum pressures. At optimum pressure of 0.23 Torr Ar (for maximum Y_{ln}), the radial inward shock wave starts from 11.5 cm and it hits on axis after 807 ns with driving magnetic piston position at 1.73 cm (Fig. 12). The incoming magnetic piston hits to the outgoing reflected shock (RS) wave after 1002 ns at 1.46 cm and the pinch starts to compress radially inward directions. During this time, the strong plasma emission especially line radiation (30 kJ) with power 3.53×10^{13} W exceeds the Joule heating energy (9.1 kJ) with power 8.81×10^{10} W causes the sharp drop of pinch radius to its minimum value of 0.14 cm at 1170 ns and then radiatively-enhanced compression occurs. At the optimum pressure, for total plasma emission, the radial inward shock wave starts at the same radial position of 11.5 cm for N_2, O_2, and Ar (Fig. 13). The starting time of the pinch and its radial position for N_2, O_2, and Ar are (1260 ns, 2.17 cm), (1080 ns, 1.85 cm), and (660 ns, 1.80 cm), respectively. The time of squeezing with the minimum pinch radius of N_2 (1980 ns), O_2 (1690 ns), and Ar(991 ns). It is clear that the sharp drop of pinch radius in Ar plasma is occurred at an earlier time from the start of radial phase than those of N_2 and O_2 plasmas leading the greatest plasma emission. Although the Lee code does not specifically include all possible phenomena which may take place during plasma focus discharges (such as filamentation, hotspots, instabilities etc), all energy- and mass-significant mechanisms are in effect incorporated in the code through the sets of mass and current factors. These mass and current factors are fitted from measured current waveforms. Hence, the Lee code is consistent with actual plasma focus operation and in particular gives reliable estimates of dynamics and radiation yields. This has been proven in comparison with many experiments over a range of small to large plasmas focus devices [42–47].

4. Conclusions

The plasma emission optimization studies in a PF device in a wide range of pressure is one of the active fields of plasma focus research for their immense possible applications. Using the Lee code, we compute bremsstrahlung radiation, line radiation, and radiative recombination with pressure variation for N_2, O_2, and Ar gases in the PF1000 device. We see that at the beginning of the pressure increase, the plasma emission starts to rise until some optimum pressure and after that it reduces with further pressure increase for each of the gases.

In our present studies, it is found that the line radiation is predominant compared to bremsstrahlung radiation and radiative recombination. Here, the maximum line radiations at their corresponding optimum pressures are as: 3.9 kJ at 0.945 Torr N_2, 6.2 kJ at

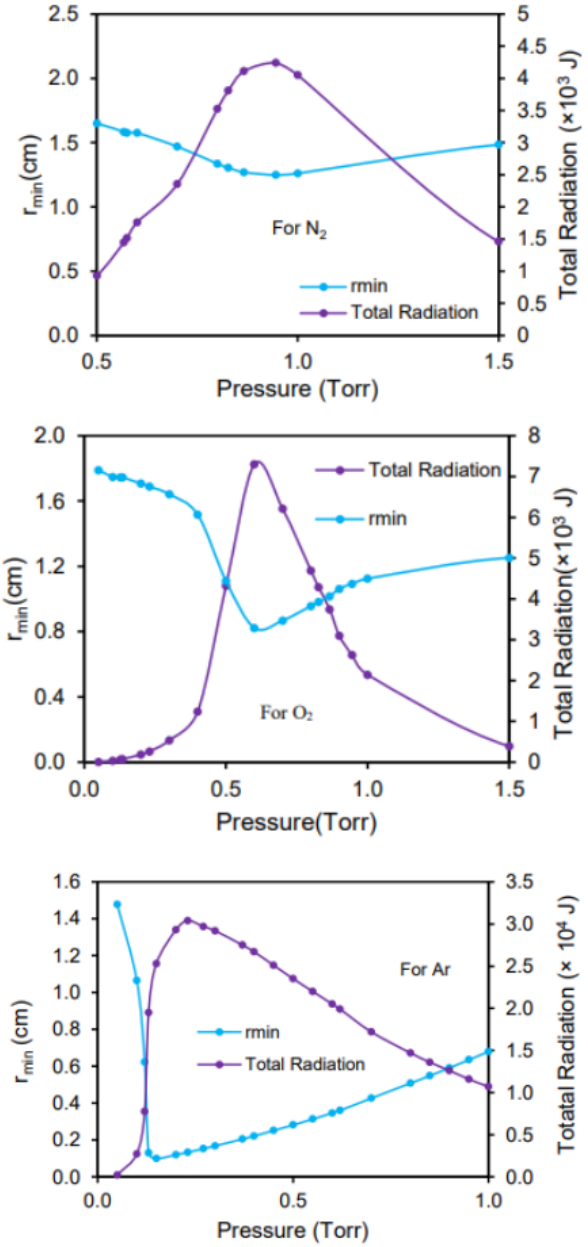

Figure 11. Minimum pinch radius and total radiation for N_2, O_2, and Ar with pressure in PF1000.

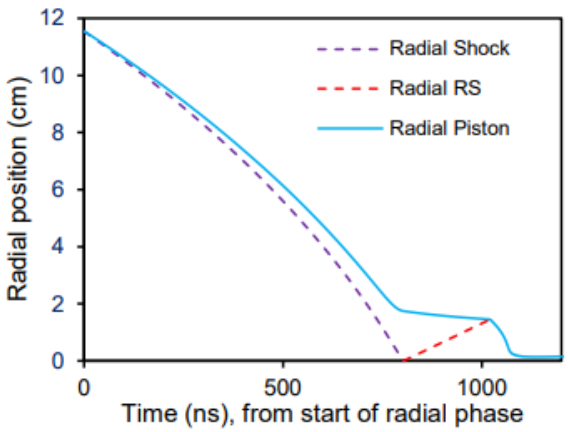

Figure 12. Radial dynamics at 0.23 Torr Ar.

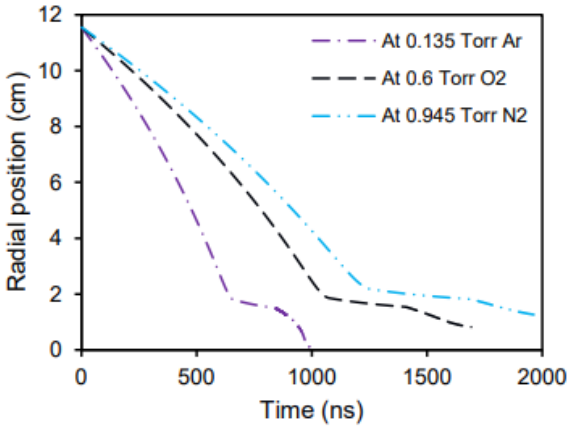

Figure 13. Radial trajectories for N_2, O_2, and Ar.

0.6 Torr O_2, and 30 kJ at 0.23 Torr Ar. The line radiation has the highest percentage (91 % for N_2, 85 % for O_2, and 97 % for Ar) within the plasma emission compared to bremsstrahlung radiation (0.98 % for N_2, 1.08 % for O_2, and 0.09 % for Ar) and radiative recombination (8 % for N_2, 14 % for O_2, and 3 % for Ar). Through the numerical studies we find the inequality relation in $r_{\min}$: $r_{\min}(N_2) > r_{\min}(O_2) > r_{\min}$ (Ar), in N_i : $N_i(\mathrm{Ar}) > N_i(O_2) > N_i(N_2)$, $T_{\max}$: $T_{\max}(\mathrm{Ar}) > T_{\max}(O_2) > T_{\max}(N_2)$, and consequently in Q_{total} : $Q_{\mathrm{total}}(\mathrm{Ar}) > Q_{\mathrm{total}}(O_2) > Q_{\mathrm{total}}(N_2)$. That means the reduction in $r_{\min}$, the increase in ion density results higher up the plasma emission. There is found a maximum Joule heating (9.1 kJ) at the optimum pressure of 0.23 Torr Ar at which it shows the peak line radiation. The excess of line radiation (20.4 kJ) as well as the lowest value of $r_{\min}$, the highest values of N_i and $T_{\max}$ of Ar are the strong evidence of radiatively-enhanced compressions.

Acknowledgements

The author acknowledges Physics discipline and Research and Innovation Centre, Khulna University for giving sound environment and active support during this research work. The author also would like to thank Director General of the Atomic Energy Commission of Syria, for encouragement and permanent support.

References

[1] S. Lee. A sequential plasma focus. *IEEE transactions on plasma science*, 19(5):912–919, 1991. doi:10.1109/27.108433.

[2] M. Mathuthu, T. G. Zengeni, and A. V. Gholap. Measurement of magnetic field and velocity profiles in 3.6 kJ United Nations University/International Center for Theoretical Physics plasma focus fusion device. *Physics of Plasmas*, 3(12):4572–4576, 1996. doi:10.1063/1.871583.

[3] G. Decker, W. Kies, and G. Pross. Experiments solving the polarity riddle of the plasma focus. *Physics*

Letters A, 89(8):393–396, 1982. doi:10.1016/0375-9601(82)90331-0.

[4] M. Sumini et al. Dose-current discharge correlation analysis in a Mather type Plasma Focus device for medical applications. *Radiation Physics and Chemistry*, 140:452–457, 2017. doi:10.1016/j.radphyschem.2017.03.022.

[5] M. Sumini, L. Isolan, M. Cremonesi, and C. Garibaldi. A plasma focus device as ultra-high dose rate pulsed radiation source. Part I: Primary electron beam characterization. *Radiation Physics and Chemistry*, 162:1–11, 2019. doi:10.1016/j.radphyschem.2019.02.027.

[6] J. Jain et al. Characterization of x-rays pulses from a hundred joules plasma focus to study its effects on cancer cells. *Journal of Physics: Conference Series*, 720(1):012043, 2016. doi:10.1088/1742-6596/720/1/012043.

[7] F. Buontempo et al. Enhancing radiosensitivity of melanoma cells through very high dose rate pulses released by a plasma focus device. *PLoS One*, 13(6):0199312, 2018. doi:10.1371/journal.pone.0199312.

[8] J. Jain et al. Hundred joules plasma focus device as a potential pulsed source for in vitro cancer cell irradiation. *AIP Advances*, 7(8):085121, 2017. doi:10.1063/1.4994655.

[9] H. S. Poh et al. Potential use of plasma focus radiation sources in superficial cancer therapy. *Japanese Journal of Applied Physics*, 59:SHHB06, 2020. doi:10.35848/1347-4065/ab7c10.

[10] V. A. Gribkov, A. Srivastava, P. L. C. Keat, et al. Operation of NX2 dense plasma focus device with argon filling as a possible radiation source for micro-machining. *IEEE transactions on plasma science*, 30(3):1331–1338, 2002. doi:10.1109/TPS.2002.802156.

[11] V. A. Gribkov, M. Liu, P. L. C. Keat, et al. Dense plasma focus radiation source for microlithography and micromachining. In *Microlithographic Techniques in Integrated Circuit Fabrication II*, volume 4226, pages 151–159. International Society for Optics and Photonics, 2000. doi:10.1117/12.404852.

[12] S. M. P. Kalaiselvi, T. L. Tan, A. Talebitaher, et al. Low-energy repetitive plasma focus based neon soft x-ray lithography source. In *Advances in X-Ray/EUV Optics and Components IX*, volume 9207, pages 160–171. SPIE, 2014. doi:10.1117/12.2062549.

[13] R. R. Prasad, M. Krishnan, K. Berg, et al. Neon dense plasma focus point x-ray source for/spl les/0.25/spl mu/m lithography. In *Proceedings of 1994 IEEE 21st International Conference on Plasma Sciences (ICOPS)*, pages 132–132. IEEE, 1994. doi:10.1109/PLASMA.1994.588868.

[14] S. M. P. Kalaiselvi, T. L. Tan, A. Talebitaher, et al. Optimization of neon soft X-rays emission from 200 J fast miniature dense plasma focus device: A potential source for soft X-ray lithography. *Physics letters A*, 377(18):1290–1296, 2013. doi:10.1016/j.physleta.2013.03.023.

[15] S. Bing. *Comparative study of dynamics and X-ray emission of several plasma focus devices*. PhD Thesis Physics Division. School of Science Nanyang Technological University, 2000.

[16] R. Baghdadi, R. Amrollahi, G. R. Etaati, et al. Characterization of the soft x-ray emission from the APF plasma focus device operated in neon. *Journal of fusion energy*, 30(2):137–143, 2011. doi:10.1007/s10894-010-9362-3.

[17] A. Roomi et al. The effect of applied voltage and operating pressure on emitted X-ray from nitrogen (N2) gas in APF plasma focus device. *Journal of fusion energy*, 30(5):413–420, 2011. doi:10.1007/s10894-011-9395-2.

[18] K. M. Ahmed, T. M. Allam, H. A. El-Sayed, et al. Numerical experiments to optimize argon soft x-ray yield in a low-energy plasma focus. *IEEE transactions on plasma science*, 47(6):2790–2800, 2019. doi:10.1109/TPS.2019.2914732.

[19] F. N. Beg et al. Study of X-ray emission from a table top plasma focus and its application as an X-ray backlighter. *J. Appl. Phys.*, 88(6):3225–3230, 2000. doi:10.1063/1.1287220.

[20] H. Bhuyan, S. R. Mohanty, N. K. Neog, et al. Comparative study of soft x-ray emission characteristics in a low energy dense plasma focus device. *J. Appl. Phys.*, 95(6):2975–2981, 2004. doi:10.1063/1.1647269.

[21] M. Zakaullah et al. Characteristics of x-rays from a plasma focus operated with neon gas. *Plasma Sources Science and Technology*, 11(4):377, 2002. doi:10.1088/0963-0252/11/4/303.

[22] M. S. Rafique, P. Lee, A. Patran, et al. Radiation emission correlated with the evolution of current sheath from a deuterium plasma focus. *Journal of fusion energy*, 29(3):295–304, 2010. doi:10.1007/s10894-010-9276-0.

[23] S. Lee, S. H. Saw, L. Soto, et al. Numerical experiments on plasma focus neutron yield versus pressure compared with laboratory experiments. *Plasma Physics and Controlled Fusion*, 51(7):075006, 2009. doi:10.1088/0741-3335/51/7/075006.

[24] S. Lee. Plasma focus radiative model: Review of the Lee model code. *Journal of Fusion Energy*, 33(4):319–335, 2014. doi:10.1007/s10894-014-9683-8.

[25] M. Akel, S. Al-Hawat, and S. Lee. Numerical experiments on soft X-ray emission optimization of nitrogen plasma in 3 kJ plasma focus SY-1 using modified Lee model. *Journal of Fusion Energy*, 28(4):355–363, 2009. doi:10.1007/s10894-009-9203-4.

[26] S. Lee et al. A simple facility for the teaching of plasma dynamics and plasma nuclear fusion. *American Journal of Physics*, 56(1):62–68, 1988. doi:10.1119/1.15433.

[27] S. H. Saw, P. C. K. Lee, R. S. Rawat, and S. Lee. Optimizing UNU/ICTP PFF plasma focus for neon soft X-ray operation. *IEEE Transactions on Plasma Science*, 37(7):1276–1282, 2009. doi:10.1109/TPS.2009.2022167.

[28] S. Lee et al. High rep rate high performance plasma focus as a powerful radiation source. *IEEE Transactions on Plasma Science*, 26(4):1119–1126, 1998. doi:10.1109/27.725141.

[29] D. Wong et al. An improved radiative plasma focus model calibrated for neon-filled NX2 using a tapered anode. *Plasma Sources Science and Technology*, 16(1):116, 2006. doi:10.1088/0963-0252/16/1/016.

[30] P. Gautam, R. Khanal, S. H. Saw, and S. Lee. Comparison of measured soft X-ray yield versus pressure for NX1 and NX2 plasma focus devices against computed values using Lee model code. *Journal of Fusion Energy*, 34(3):686–693, 2015. doi:10.1007/s10894-015-9872-0.

[31] V. Siahpoush, M. A. Tafreshi, S. Sobhanian, and S. Khorram. Adaptation of Sing Lee's model to the Filippov type plasma focus geometry. *Plasma Physics and Controlled Fusion*, 47(7):1065, 2005. doi:10.1088/0741-3335/47/7/007.

[32] S. Lee, S. H. Saw, P. Lee, and R. S. Rawat. Numerical experiments on plasma focus neon soft X-ray scaling. *Plasma Physics and Controlled Fusion*, 51(10):105013, 2009. doi:10.1088/0741-3335/51/10/105013.

[33] M. Akel and S. Lee. Practical optimization of AECS PF-2 plasma focus device for argon soft X-ray operation. *Journal of Fusion Energy*, 31(2):122–129, 2012. doi:10.1007/s10894-011-9444-x.

[34] Y. Ay. Spherical plasma focus operated with nitrogen and neon gases for soft x-rays (bremsstrahlung radiation, line radiation, and radiative recombination). *Plasma Physics and Controlled Fusion*, 63(7):075011, 2021. doi:10.1088/1361-6587/abf22f.

[35] M. Akel, S. Ismael, S. Lee, et al. PF1000 high-energy plasma focus device operated with neon as a copious soft X-ray source. *IEEE Transactions on Plasma Science*, 45(11):2979–2983, 2017. doi:10.1109/TPS.2017.2761843.

[36] M. Akel and S. Lee. Radiative collapse in plasma focus operated with heavy noble gases. *Journal of Fusion Energy*, 32(1):111–116, 2013. doi:10.1007/s10894-012-9535-3.

[37] V. A. Gribkov et al. Plasma dynamics in the PF-1000 device under full-scale energy storage: II. Fast electron and ion characteristics versus neutron emission parameters and gun optimization perspectives. *Journal of Physics D: Applied Physics*, 40(12):3592, 2007. doi:10.1088/0022-3727/40/12/008.

[38] M. Akel, S. Ismael, S. Lee, et al. Numerical experiments on the PF1000 plasma focus device operated with nitrogen and oxygen gases. *Modern Physics Letters B*, 31(16):1750167, 2017. doi:10.1142/S0217984917501676.

[39] M. Akel et al. Experiments and simulations on the possibility of radiative contraction/collapse in the PF-1000 plasma focus. *Nukleonika*, 61(2):145–148, 2016. doi:10.1515/nuka-2016-0025.

[40] S. Lee, S. H. Saw, and J. Ali. Numerical experiments on radiative cooling and collapse in plasma focus operated in krypton. *Journal of Fusion Energy*, 32(1):42–49, 2013. doi:10.1007/s10894-012-9522-8.

[41] M. Akel, A. Kulińska, S. Lee, et al. Results of plasma radiative compression investigation in the PF-24 device operated with D2, Ar and (100using the 5-phase Lee model code. *JApplied Radiation and Isotopes*, 182(6):110118, 2022. doi:10.1016/j.apradiso.2022.110118.

[42] P. Kubes et al. The evolution of the plasmoidal structure in the pinched column in plasma focus discharge. *Plasma Physics and Controlled Fusion*, 58(4):045005, 2016. doi:10.1088/0741-3335/58/4/045005.

[43] P. Kubes et al. Characteristics of closed currents and magnetic fields outside the dense pinch column in a plasma focus discharge. *Physics of Plasmas*, 27(9):092702, 2020. doi:10.1063/5.0010249.

[44] P. Kubes et al. Scenario of a magnetic dynamo and magnetic reconnection in a plasma focus discharge. *Matter and Radiation at Extremes*, 5(4):046401, 2020. doi:10.1063/1.5133103.

[45] N. Benett et al. Kinetic simulations of gas breakdown in the dense plasma focus. *Physics of Plasmas*, 24(6):062705, 2017. doi:10.1063/1.4985313.

[46] E. N. Hahn et al. Effect of insulator length and fill pressure on filamentation and neutron production in a 4.6 kJ dense plasma focus. *Physics of Plasmas*, 29(8):083508, 2022. doi:10.1063/5.0087901.

[47] C. Pavez and L. Soto. Demonstration of X-ray emission from an ultraminiature pinch plasma focus discharge operating at 0.1 J nanofocus. *IEEE Trans. Plasma Sci.*, 38(5):1135, 2010. doi:10.1109/TPS.2010.2045110.